Enhancing efficacy of gemcitabine in pancreatic patient-derived xenograft mouse models

Andriana Inkoom[a], Nkafu Ndemazie[a], Kevin Affram[a], Taylor Smith[a], Xue Zhu[a], Patrick Underwood[b], Sunil Krishnan[c], Edward Ofori[d], Bo Han[e], Jose Trevino[b], Edward Agyare[a,*]

[a] College of Pharmacy and Pharmaceutical Sciences, Florida A & M University, Tallahassee, FL, United States of America
[b] University of Florida Department of Surgery, Gainesville, FL, United States of America
[c] Mayo Clinic, Jacksonville, FL, United States of America
[d] College of Pharmacy, Chicago State University, Chicago, IL, United States of America
[e] Department of Surgery, Keck School of Medicine University of Southern California, Los Angeles, United States of America

ARTICLE INFO

ABSTRACT

Gemcitabine (Gem), a nucleoside analog, is a preferred choice of treatment for pancreatic cancer (PCa) and often used in combination therapy against wide range of solid tumors. It is known to be rapidly inactivated in blood by cytidine deaminase. The objective of the study was to improve the systemic stability and anticancer activity of modified Gem termed 4-N-stearoylGem (4NSG) In this study, the IC_{50} values of 4NSG treated MiaPaCa-2 and primary pancreatic cancer (PPCL-46) cultures were significantly lower when compared with gemcitabine hydrochloride (GemHCl) treated cultures. In acute toxicity study, liver enzyme level of aspartate aminotransferase (AST) of the control mice was not significantly different from AST levels of 4NSG and GemHCl treated mice. However, alanine aminotransferase (ALT) level of control mice (67 ± 5 mUnits/mL) was significantly lower compared with ALT levels of GemHCl (232 ± 28 mUnits/mL) and that of 4NSG (172 ± 22 mUnits/mL) ($p < 0.0001$). More importantly, ALT level of 4NSG was lower than ALT level of GemHCl ($p < 0.05$). Although ALT levels were elevated, pathological images of liver and kidney tissues of control, GemHCl and 4NSG treated mice revealed no architectural changes and no significant change in mice weight was observed during treatment. The bioavailability (AUC) of 4NSG was 3-fold high and significantly inhibited the tumor growth as compared with equivalent dose of GemHCl. Immunohistochemical staining revealed that 4NSG significantly inhibited the expression vascular endothelial growth factor (VEGF) receptor. The study is unique because it established, for the first time, enhanced anticancer activity of 4NSG against pancreatic patient-derived xenograft (PDX) mouse model and PPCL-46 cells compared with Gem. 4SGN enhanced pharmacokinetic profile and improved the therapeutic efficacy of the standard-of-care Gem. Lastly, 4GSN showed a remarkable tumor growth inhibition and revealed significant antiangiogenic activity in 4GSN treated pancreatic PDX tumor.

1. Introduction

Pancreatic cancer (PCa) is one of the most aggressive and devastating type of malignancies in the United States of America with high mortality rate (Siegel et al., 2019). It is expected to surpass breast and colorectal cancer in the next two years to become the second leading cause of cancer-related deaths (Siegel et al., 2019; Grasso et al., 2017). The 5-year survival rate of 5% is one of the poorest according to World Health Organization (WHO) (Binenbaum et al., 2015). Although we live in an era filled with remarkable advances in cancer treatment, there are limited therapeutic options for patients diagnosed with PCa. Gemcitabine (Gem), a nucleoside analog, has been in existence for more than a

decade and remains the first-choice treatment for PCa. However, Gem treatment resistance coupled with its poor pharmacokinetic profile (short half-life) has resulted in poor treatment outcomes (de Sousa Cavalcante and Monteiro, 2014). Gem is given as monotherapy in patients with locally advance and metastatic PCa and a good response in the early stages of treatment, nonetheless, drug resistance develops with time (de Sousa Cavalcante and Monteiro, 2014; Jia and Xie, 2015).

Gem as a choice of drug in PCa therapy has improved the quality of life, disease related symptoms and the survival rate with unresectable PCa (Andersson et al., 2009). Standardized clinical dosing schedule for Gem given as an intravenous (IV) fusion for 30 min is 1000 mg/mg^2 administered weekly for 3 weeks (28 day cycle) followed by a week of
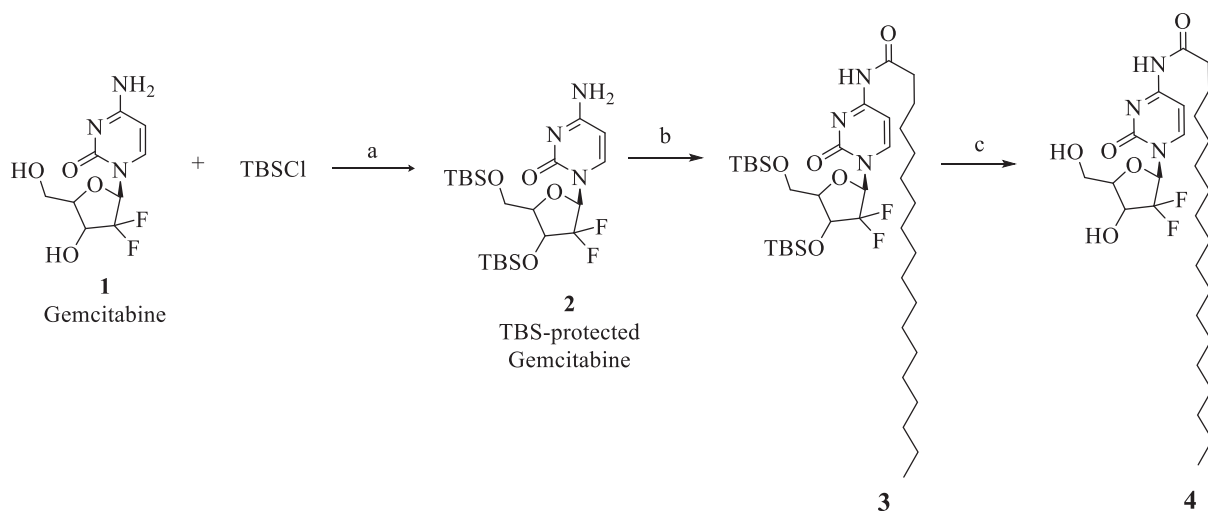
Scheme 1. Reagents and conditions for the synthesis of 4NSG (4): a) TBSCl, imidazole, DCM, rt. b) DIPEA, stearic anhydride, DCM, 24 h c) TBAF DMF, rt., 2 h.

resting phase (Garcia-Cremades et al., 2018). Gem is a cytotoxic agent with mechanism of action that involves biotransformation into triphosphate metabolite that blocks DNA synthesis (Grasso et al., 2017; Liu et al., 2018). A major concern which constrains effective therapy is systemic instability due to cytidine deaminase-induced deactivation of Gem via the removal of –NH$_2$ to yield an inactive metabolite which is excreted in urine (Amrutkar and Gladhaug, 2017). In humans, the half-life of Gem has been reported as 8–17 min as a result of the rapid metabolism (Dai et al., 2017). Further, cellular uptake and internalization of Gem depends on nucleoside transporters on the surface of PCa cells namely the human equilibrative nucleoside transporter 1 (hENT1) which often times are under-expressed in more than 65% of PCa patients (Dai et al., 2017). Another challenge of concern is that, PCa cells are besieged by a thick desmoplastic stromal matrix and has been implicated in drug resistance (Mei et al., 2016). It is justified to say that the ability to surmount this thick biological barrier will arguably improve drug delivery and efficacy in cancer chemotherapy.

There has been a growing interest in the applications of modified existing chemotherapeutic agents and patient derived tumor xenografts in cancer research, a paradigm shift from chemotherapy drugs and conventional cancer cell lines (Hidalgo et al., 2014; Jin et al., 2010). In this study, we successfully synthesized 4NSG from Gem and stearic acid. We conducted cytotoxicity and apoptotic studies of 4NSG on MiaPaCa-2 and PPCL-46 cells. Tumor efficacy studies were performed in mice bearing pancreatic PDX tumor. In this study, we demonstrated that synthesized 4NSG remarkably reduced tumor growth in pancreatic PDX mouse model due to increased bioavailability and reduced vascular endothelial growth factor (VEGF) receptors expression while histological data revealed no morphological changes in liver and kidney tissues among the control, GemHCl and 4NSG treated PDX mouse model. Put together, the current study is novel because it discovered, for the first time, enhanced anticancer activity of 4NSG against pancreatic patient-derived xenograft (PDX) mouse model and PPCL-46 cells compared with Gem. Secondly, 4SGN enhanced pharmacokinetic profile and improved the therapeutic efficacy of the standard-of-care Gem. Thirdly, 4GSN showed a remarkable tumor growth inhibition and revealed significant antiangiogenic activity in 4GSN treated pancreatic PDX tumor.

2. Materials and methods

2.1. Materials

Gemcitabine Hydrochloride (GemHCl) was purchased from AK Scientific (Union City, CA). Pancreatic cancer MiaPaCa-2 cells (K-Ras

(G12C)) were bought from American Type Culture Collection (ATCC) (Manassas, VA). PPCL-46 is a patient-derived cell line (K-Ras (G12V)) obtained from Dr. Trevino's laboratory with methods previously described (Pham et al., 2016). The PPCL-46 was derived from a 75-year-old, Caucasian female with a moderately differentiated, T3N1 pancreatic ductal adenocarcinoma who underwent pancreatoduodenectomy for her disease. All materials, both solvents and reagents of analytical grade were purchased from Sigma Aldrich (St. Louis, MO).

2.2. Synthesis of 4NSG

Synthesis of 4NSG followed a method as described by Trung et al. (Trung Bui et al., 2013; Immordino et al., 2004) with slight modifications. Gemcitabine **1** (2.630 g, 9.992 mmol, 1 eq) was dissolved in 100 mL dichloromethane (50.0 mL). To the solution was added *tert*-butyldimethylsilyl (TBS) chloride (3.765 g, 24.981 mmol, 2.5 eq) and imidazole (2.041 g, 29.977 mmol, 3 eq) successively. The reaction mixture was stirred at room temperature until Gem was consumed, as indicated by thin layer chromatography (TLC) analysis (using 100% ethyl acetate (EtOAc)). The mixture was washed successively with saturated ammonium chloride, sodium bicarbonate and sodium chloride solutions. The organic layer was dried by anhydrous sodium sulfate, filtered and concentrated under vacuum. The TBS-protected compound **2** was crystalized from EtOAc as a white solid which was used in the next step without further purification (Scheme 1) (Trung Bui et al., 2013).

Next, to a solution of N, N-diisopropylethylamine (DIPEA) (1.200 eq) in dichloromethane (DCM) was added stearate anhydride (1.100 eq)-warmed to dissolve and TBS protected gemcitabine **2** (~1.000 eq). The resulting mixture was stirred for 24 h at room temperature. After, the excess solvent was removed under reduced pressure. The residue containing intermediate **3** obtained was used in the next step without further purification.

A mixture of **3** (1 g, 1.4 mmol) and tetra-n-butylammonium fluoride (TBAF) in dimethylformamide (DMF) (15 mL) was stirred at room temperature for 2 h. Excess solvent was removed and the resulting residue was directly purified on silica gel flash column chromatography with gradient DCM-ethanol (up to 15% ethanol) to afford 4NSG (**4**) as a white solid (Trung Bui et al., 2013).

The 4NSG was synthesized according to Scheme 1 and analyzed by proton and carbon-13 NMR, elemental analysis and TLC. The melting point for solid 4NSG compound was determined. The purity of the 4NSG was close to 99.6% as determined by NMR and elemental analysis. Elemental analysis was conducted by Atlantic Microlab, Inc., Norcross, GA.

2.2.1. Preparation of 4NSG stock solution

4NSG stock solution was prepared by adding 200 mg of soy lecithin in 10 mL of sterile water. The mixture was vortexed intermittently until soy lecithin was dissolved completely followed by addition of 240 mg 4NSG to soy lecithin solution. The mixture was sonicated until 4NSG dispersed completely in the solution (Kumar et al., 2014; Zhang et al., 2018). Soybean lecithin is a basic substance of life, and it is a safe natural mixture of phospholipids (Kumar et al., 2014). It exhibits an amphiphilic structure which may be used as an inactive ingredient and its FDA approved.

4NSG.
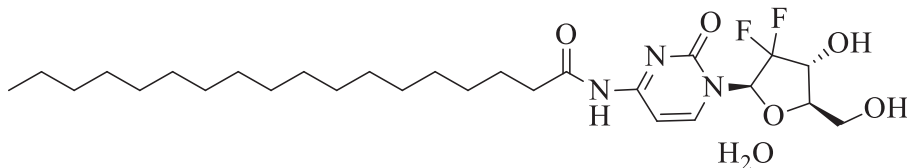
^{1}H NMR (600 MHz, DMSO-d_6) δ 10.93 (s, 1H), 8.20 (d, J = 7.6 Hz, 1H), 7.25 (d, J = 7.7 Hz, 1H), 6.27 (d, J = 6.5 Hz, 1H), 6.14 (t, J = 7.4 Hz, 1H), 5.27–5.24 (m, 1H), 4.19–4.14 (m, 1H), 3.86 (d, J = 8.4 Hz, 1H), 3.80–3.75 (m, 1H), 3.65–3.59 (m, 1H), 2.40–2.34 (m, 2H), 1.51 (t, J = 7.4 Hz, 2H), 1.26–1.15 (m, 28H), 0.82 (t, J = 7.0 Hz, 3H).

^{13}C NMR (151 MHz, DMSO) δ 174.53, 163.33, 154.64, 145.16, 123.38, 96.34, 84.55, 81.47, 68.83, 59.23, 36.83, 31.72, 29.46, 29.44, 29.42, 29.40, 29.27, 29.13, 28.87, 24.78, 22.52, 14.38. **MP** = (145-146 ˚C), **Rf** value = 0.54 (100% ethyl-acetate). HPLC (H$_2$O/ACN (90:10), % purity = 99.8%, RT = 14.3 min) MS (M + H)$^+$ = 530.59, Molecular formula: $C_{27}H_{45}F_2N_3O_5$•H_2O, Mol wt: 547.68. Elemental Analysis: Calculated, C, 59.21H, 8.65 N, 7.67 F, 6.94; Found, C, 59.27; H, 8.59; N, 7.51; F, 6.67.

2.3. Cytotoxicity in two and three dimensional (2D and 3D) cultures 2D MiaPaCa-2 and PPCL-46 cells

Prior to viability studies, Dulbecco's modified Eagle medium (DMEM) with high glucose and L-glutamine was supplemented with 10% fetal bovine serum (FBS) and 1% penicillin-streptomycin (PenStrep) (Vande Voorde et al., 2019). Briefly, MiaPaCa-2 and PPCL-46 were seeded at a density of 1×10^3 per well in 96-well plates in triplicates for each drug concentration level and incubated at 5% CO$_2$ and temperature of 37 ˚C (Vande Voorde et al., 2019). At 70–75% confluence, both MiaPaCa-2 and PPCL-46 cells were treated with GemHCl and 4NSG. Varying concentrations of 4NSG was prepared from its stock solution with growth medium. For GemHCl, a stock solution was prepared with phosphate-buffered saline (PBS) and serially diluted with growth medium to prepare varied concentrations: thus 5, 10, 20, 40 and 60 µM. Both cells were treated with 100 µL of each drug concentration in triplicates and incubated for 48 h. At termination, 20 µL of 0.05% resazurin sodium salt (Alamar blue®) was added and incubated at optimum conditions (5% CO$_2$, 37 ˚C) for 4 h (Gradiz et al., 2016). Fluorimetric analysis was determined at excitation wavelength of 560/580 nm and emission wavelength of 590/610 nm and the percent viable cells per concentration calculated.

2.4. 3D Spheroid of MiaPaCa-2 and PPCL-46 cells

MiaPaCa-2 and PPCL-46 cells were plated in 3D formation 96-well plates, Nunclon Sphera® at seeding density of 3.0×10^4 and 2.6×10^4 in 100 µL/well of growth medium respectively, volume of cell suspension in each well plate was then made up to 200 µL with growth medium and incubated for 72 h to allow for spheroid formation (Paskeviciute and Petrikaite, 2017). At treatment, 100 µL of supernatant was replaced with drug in growth medium prepared as described under 2D viability studies of MiaPaCa-2 and PPCL-46 cells and incubated for 48 h (Wen et al., 2013). At termination, 50 µL of 0.05% resazurin sodium salt (Alamar blue®) was added to each well and gently dispersed by pipetting and incubated for 4 h. Fluorimetric analysis was measured as described above (Wen et al., 2013; Diaz Osterman et al., 2016).

2.5. 4NSG induced apoptosis

PPCL-46 cells were seeded in 96-well plates at a density of 1.0×10^3 cells/well and incubated at optimum conditions until the cells reached 70–75% confluency. At confluency, the cells were treated with Gem (with Gem equivalent dose of GemHCl and 4NSG) at a concentration of 20, 40 and 80 µM. Briefly, the cells were treated for 24 h, washed twice with PBS and fixed with 4% formalin for 15–20 min. Afterwards, the cells were permeated with 0.1% Triton-X for 15 mins and finally incubated with 20 µL mixture of 5 µg acridine orange (AO)/3 µg ethidium bromide (EB) (ratio 1:1) and kept away from light for 30 min (Liu et al., 2015). Cells were finally washed thrice with sterile PBS and examined for evidence of apoptosis under an Olympus fluorescence microscope.

2.6. Animals

Eight-week-old female non-obese diabetic (Cg-Prkdc^{scid}Il2rg^{tm1Wjl}/SzJ (NSG) mice were obtained from The Jackson Laboratory (Bar Harbor, ME).

2.6.1. Ethics statements

The mice were housed in a virus-free, indoor, light- and temperature- controlled barrier environment, and were provided ad libitum access to food and water. All procedures with mice were in strict accordance with the National Institutes of Health Guide for the Care and Use of Laboratory Animals and approved by the Florida A & M University Animal Care and Use Committee.

2.6.2. Tumor transplantation

The implantation of surgical tumor tissue into immuno-compromised mice was described previously (Pham et al., 2016; Delitto et al., 2015). Briefly, a viable portion of resected tissue 2 × 2 mm in size was isolated immediately from surgically resected primary PCa specimens with care to minimize critical ischemia time. PCa tissue was then implanted subcutaneously into an 8-week-old female non-obese diabetic Cg-Prkdc^{scid}Il2rg^{tm1Wjl}/SzJ (NSG) mouse (The Jackson Laboratory, Bar Harbor, ME). Xenografts were allowed to grow to a maximum diameter of 1.5 cm before passage and/or in vitro culture. Herein, we defined a passage as explanation of a PCa xenograft and implantation into the flank of a new host.

2.7. Pharmacokinetic studies

For pharmacokinetic (PK) studies, normal healthy mice were grouped into control, GemHCl and 4NSG. Mice were given a single bolus intravenous injection of 30 mg/kg of Gem (with Gem equivalent dose of GemHCl and 4NSG) while control mice received normal saline (0.9% NaCl). After the injection, aliquots of blood samples were collected at predetermined time points (5, 10, 15, 30, 60, 120, 240, 360, 720 and 1440 min). Blood samples collected were treated with 2 mL of an extraction solvent (15% of isopropyl alcohol in ethyl acetate) (Beumer et al., 2008; Affram et al., 2017). The mixture was vortexed for 30 s and centrifuged at 3000 rpm for 15 and the supernatant collected and vaporized to dry overnight in a water-bath. Residual solvent was removed by placing the dried samples in the vacuum chamber. Finally, 500 uL of mobile phase was used to reconstitute the dried sample (5% acetonitrile in 10 mM dihydrogen phosphate buffer, pH adjusted to 3). The sample solution was again centrifuged at 3000 rpm for 15 min, supernatant collected and filtered and samples analyzed for Gem by HPLC-UV (Apparaju et al., 2008). The PK parameters were estimated by using PKSolver (Zhang et al., 2010).

2.7.1. HPLC analysis

Gem analysis was performed according to method described by Lanz and colleagues with minor modifications (Lanz et al., 2007). Briefly, Gem analysis was performed using a chromatographic system, which consisted of a HPLC (Waters Corporation, Milford, MA) equipped with an auto-sampler, photo diode array (2998 UV/Vis) detector and pumps. Separation was performed using a reverse phase column (ZORBEX SB – C18 4.6 × 250 mm, 5 μm). A flow rate of 1.0 mL/min and injection volume 20 μL at ambient temperature were maintained while detection was performed at 268 nm. Prior to analysis, reverse phase column was equilibrated with mobile phase made up of 5% acetonitrile in 10 mM dihydrogen phosphate buffer, pH adjusted to 3 with trifluoroacetic acid (TFA). An isocratic elution was performed throughout the entire analysis including internal standards.

A calibration curve was prepared using Gem standard solutions with concentration range of 0.063–2.0 μg/mL. A plot of the peak areas as a function of Gem concentration was plotted and the linear equation of the calibration curve given as y = mx + c was determined, where y is the peak area, m is the slope, x is the concentration of Gem and c is the y - intercept was. Supernatants from controls were spiked with aliquots of 0.5 μg/mL of Gem. Recovery of Gem in supernatant from blood and tissues was performed by comparing peak areas of controls spiked with known amounts of Gem (Lanz et al., 2007).

2.8. Acute toxicity studies

2.8.1. Histology

Histological studies were performed in normal healthy mice to assess the integrity of the liver and kidney tissues after the single bolus intravenous administration of 30 mg/kg of Gem (with Gem equivalent dose of GemHCl and 4NSG). Two weeks after the administration, mice were euthanized and the liver and kidneys extracted. The wet tissues were rinsed in PBS, submerged in 10% neutral buffered formalin (NBF) and stored for 48 h at room temperature.

Tissue examination: In the final step liver and kidney tissues were embedded in paraffin wax to prepare blocks. Tissue sections of 5 μm thickness were cut and hematoxylin and eosin (H&E) stained and examined under light microscope (Krishna, 2013).

2.8.2. Liver enzymes activity

Twenty-four hours after administration of 30 mg/kg of Gem (Gem equivalent dose of GemHCl and 4NSG) to normal healthy mice, blood samples were collected in the control, GemHCl and 4NSG treated groups. This study was conducted to determine any elevation of key liver enzymes includingaspartate aminotransferase (AST) and alanine aminotransferase (ALT) activity using reagent kits from Sigma-Aldrich (catalogue # MAK055 for AST; catalogue # MAK052 for ALT) (Ricart, 2017). The manufacturer's assay procedure was followed with minor modifications. Briefly, the collected blood samples were centrifuged at 3500 rpm for 6 min the serum was collected, and then serially diluted.

In the assay of AST activity, standard glutamate solution was used to plot a calibration curve. Briefly, 10 μL of 0.1 M glutamate standard solution was diluted with 990 μL of AST assay buffer to produce a 1.0 mM stock solution. The stock solution was serially diluted with AST assay buffer to yield standard solutions of 0 (blank), 2, 4, 6, 8, 10 nmole/well in a 96-well plate. As a guide, a positive control was also included in this assay by adding 5 μL of AST positive control and diluted with 45 μL with AST assay buffer. For the samples, a master reaction mix was prepared per the manufacturer's protocol using a scale factor of 20; AST enzyme buffer = 1600 μL, AST enzyme mix = 40, AST developer = 160 μL and AST substrate = 200 μL.

Fifty microliters of serially diluted solutions of control, GemHCl and 4NSG were pipetted in triplicates and in 96-well plate, diluted with 100 μL master reaction mix and mixed well by pipetting. Plates were protected away from light by wrapping them in aluminum foils. Subsequently, the plates were incubated at 37 °C for 3 mins and the absorbance measured on a Bio-Rad iMark™ Microplate reader at 450 nm as the initial absorbance ($A_{initial}$) and time recorded as $T_{initial}$. Absorbance recordings were taken every 5 min until the most active sample gave an absorbance that exceeds the highest glutamate standard (10 nmole/well). The penultimate reading (A_{final} at T_{final}) thus reading before the linear range of the calibration curve was used to calculate the AST activity. The change in absorbance ($A_{final} - A_{initial}$) was calculated and the glutamate activity determined from the calibration curve. The AST activity was determined from the equation provided below.

$$AST\ Activity = \frac{B \times Sample\ dilution\ factor}{Reaction\ time \times Sample\ volume\ (mL)} \quad (1)$$

where B = Amount (nmole) of glutamate generated between Tinitial and Tfinal.

Reaction time = Tfinal – Tinitial in minutes.

In the estimation of ALT activity, the same procedure above was repeated, however, the calibration curve was generated with a pyruvate standard and serial dilutions were done with an ALT assay buffer provided by the kit. The master reaction mix was prepared as shown; ALT assay buffer = 1548 μL, fluorescent peroxidase substrate = 36 μL, ALT enzyme mix = 36 μL and ALT substrate = 180 μL.

Absorbance was measured in a similar manner as described in the assay of AST activity. In lieu, measurement was performed at 595 nm and the change in absorbance calculated similarly to AST assay. The ALT activity was calculated as provided below.

$$ALT\ Activity = \frac{B \times Sample\ dilution\ factor}{Reaction\ time \times Sample\ volume\ (ml)} \quad (2)$$

B = Amount (nmole) of pyruvate generated between Tinitial and T final.

2.9. Immunohistochemistry

Mice were euthanized and tissue samples (tumor, liver and kidney) were excised from mice immediately, washed with PBS and placed in 10% buffered formalin for 24 h and transferred to 70% ethanol for histopathological analysis. Histology was performed by HistoWiz Inc. (histowiz.com) using a Standard Operating Procedure and fully automated workflow. Samples were processed, embedded in paraffin, and sectioned at 4 μm (Harder et al., 2009; Pignochino et al., 2010; Walsh et al., 2013). Immunohistochemistry was performed on a Bond Rx autostainer (Leica Biosystems) with enzyme treatment (1:1000) using standard protocols. Antibodies used were rat monoclonal F4/80 primary antibody (eBioscience, 14–4801, and 1:200) and rabbit anti-rat secondary (Vector, 1:100) (Harder et al., 2009; Pignochino et al., 2010;

Walsh et al., 2013). Bond Polymer Refine Detection (Leica Biosystems) was used according to manufacturer's protocol. After staining, sections were dehydrated and film coverslipped using a Tissue-Tek Prisma and Coverslipper (Sakura). Whole slide scanning (40×) was performed on an Aperio AT2 (Leica Biosystems).

2.10. Tumor efficacy studies

In this study, mice bearing surgically implanted tumor mice with sizes of 70–100 mm^3 were randomized into groups as control, GemHCl and 4NSG ($n = 5$/group). Baseline tumor volumes were established and dosing initiation began on day 1 with intravenous administration of 30 mg/kg Gem (twice weekly for 3 weeks) with equivalent dose of GemHCl and 4NSG (Li et al., 2005). Once tumors became palpable tumor volumes were measured thrice per week and weight of mice recorded twice per week. Tumor volumes were measured using calipers and calculated using the following equation: $V = (L*(W)^2)/2$, where V is volume (mm^3), W(width) is the smaller of two perpendicular tumor axes and the value L (length) is the larger of two perpendicular axes. Mean tumor volume growth curves and means were calculated for each treatment group (Delitto et al., 2015).

2.11. Statistical analysis

Pharmacokinetic parameters were estimated using software PKSolver. The difference between GemHCl and 4NSG treatment groups were analyzed using Student's t-test and considered significant at $p < 0.05$. All experiments were performed at least in triplicate and analyzed using GraphPad Prism software (GraphPad Software, Inc., San Diego, CA).

3. Results

3.1. Confirmation of synthesis of 4NSG by ^{1}H NMR

We successfully synthesized 4NSG in good yields and characterized the structure using ^{1}H and ^{13}C NMR which was in-agreement with reported data (Immordino et al., 2004) (Scheme 1, Supplementary Fig. S1 A and B, Supplementary Fig. S2). Characteristic 4NSG ^{1}H NMR peaks were 10.88 ppm (-CO-NH) and 1.38–1.04 ppm (-CH$_2$-)$_{15}$ representing the amide linkage and long chain methylene group contributed by stearic acid respectively. The introduced amide carbonyl carbon in 4NSG displays a characteristic C-13 NMR peak at 174.55 ppm. These peaks confirmed the successful conjugation of stearic acid to Gem.

3.2. Cytotoxicity effect of GemHCl and 4NSG

The cytotoxic activity of the conjugate was preliminarily evaluated in MiaPaCa-2 cells via 2D culture and 3D spheroids using the Alamar blue assay. As shown in the Fig. 1A and Table 1, 4NSG demonstrated significant cytotoxic activity against 2D MiaPaCa-2 culture with IC$_{50}$ value of 27.6 ± 1.3 μM compared with GemHCl treated with after 48 h treatment by a magnitude of approximately 1.7 fold-high in 2D culture compared with GemHCl treated group with IC$_{50}$ value of 45.7 ± 1.4 μM. While IC$_{50}$ values were higher in the treated 3D MiaPaCa-2 culture compared with that of 2D MiaPaCa-2 culture (Fig. 1B and Table 1), 4NSG treated 3D MiaPaCa-2 culture (IC$_{50}$ = 39.1 ± 1.5 μM) showed high cytotoxic effect compared with GemHCl treated 3D MiaPaCa-2 culture (IC$_{50}$ = 55.8 ± 1.2 μM).

To investigate the effects of GemHCl and 4NSG on 2D and 3D PPCL-46 cultures, we exposed the cultures to varying concentrations of Gem (Gem equivalent dose of GemHCl and 4NSG). The observed cytotoxic effects of GemHCl and 4NSG against PPCL-46 cultures appeared to follow a similar trend to that of 2D and 3D MiaPaCa-2 cultures. 2D and 3D PPCL-46 cultures were more sensitive to 4NSG than GemHCl (Fig. 1 C and D, Table 1). We evaluated the performance of GemHCl and 4NSG

against the cultures, based on their IC$_{50}$ values. We found that IC$_{50}$ value (75.5 ± 1.5 μM) of GemHCl treated 2D PPCL-46 culture was significantly greater than the IC$_{50}$ value (41.0 ± 1.0 μM) of 4NSG treated 2D PPCL-46 culture. For 3D PPCL-46 cultures, IC$_{50}$ value (95.2 ± 1.4 μM) of GemHCl was markedly greater than IC$_{50}$ value (59.9 ± 1.8 μM) for 4NSG. Fig. 2 exhibits the integrity of PPCL-46 spheroids after exposure to varying concentrations of Gem (with Gem equivalent dose of GemHCl and 4NSG). Upon a careful examination of spheroid images, we observed that 4NSG treated 3D spheroid exhibited a larger surface area as the Gem concentration increases. This behavior in spheroid pattern may be attributed to loosening of cells adhesion or spheroid integrity compared with GemHCl treatment alone.

3.3. 4NSG induced apoptosis

To show the morphology of apoptosis in PPCL-46 cells upon exposure to GemHCl and 4NSG at varying Gem concentrations of 20, 40 and 80 μM (with Gem equivalent dose of GemHCl and 4NSG), acridine orange (AO) and ethidium bromide (EB) staining was performed. At higher concentrations (40 μM and 80 μM), significant number of 4NSG treated PPCL-46 cells exhibited signs of early apoptosis observed as greenish yellow florescence compared with GemHCl (merged images) Fig. 3. Late apoptosis was identified as reddish-orange fluorescence and it was observed to be more prominent in 4NSG treated cells compared with the control or GemHCl treated cells especially at Gem concentrations at 20 and 40 μM.

3.4. Acute toxicity studies

Histological studies by H and E staining was performed to investigate the cytotoxic effect of GemHCl and 4NSG on the kidney and liver tissues. Histological changes in the liver and kidney serve as evidence of injury due to drugs and possible bioaccumulation (Popescu et al., 2017). Kidney and liver sections from control mice treated with normal saline showed normal architecture of hepatic and renal cells with well-preserved cytoplasm (Fig. 4A and D). Histopathological examination of kidney (Fig. 4B and C) and liver (Fig. 5E and F) of mice treated with 30 mg/kg of Gem (Gem equivalent dose of GemHCl and 4NSG) exhibited no significant morphological changes as compared to the control group.

In Tables 2 and 3, no statistically significant elevation of AST level was observed between the control (non-treated) group and GemHCl group or the control and the 4NSG group. However, elevated level of ALT was observed in GemHCl and 4NSG groups compared with the control group. Further, ALT levels in the GemHCl treated group was markedly higher than the 4NSG treated group.

3.5. Immunohistochemistry (IHC)

Epidermal growth factor receptor (EGFR) and human EGFR 2 (HER2) and vascular endothelial growth factor receptor (VEGFR) are tyrosine kinase receptors highly expressed in several solid tumors including pancreatic cancer (Lozano-Leon et al., 2011; Karanikas et al., 2016). These receptors are frequently reported to harbor aberrant activities that may lead to proliferation, survival, migration and differentiation required for PCa pathogenesis. We therefore evaluated the impact of our novel formulated 4NSG on the expression of EGFR, HER2 and VEGFR in the mice pancreatic tumor tissue. Fig. 5 displays immunohistochemical staining of EGFR, HER2 and VEGF in PDX tumor tissues with brown regions demonstrating high positive staining. Images A, B and C show moderate EGFR expression (IHC 1+) with no clear difference in expression between GemHCl and 4NSG treated-tumor tissues (Fig. 5B and C). Similar trend of HER2 expression was observed in the tumor tissues where high HER2 expression (IHC 2+) was displayed in control (untreated), GemHCl and 4NSG treated tumor tissues (Fig. 5D, E and F). For VEGF receptor expression, control and
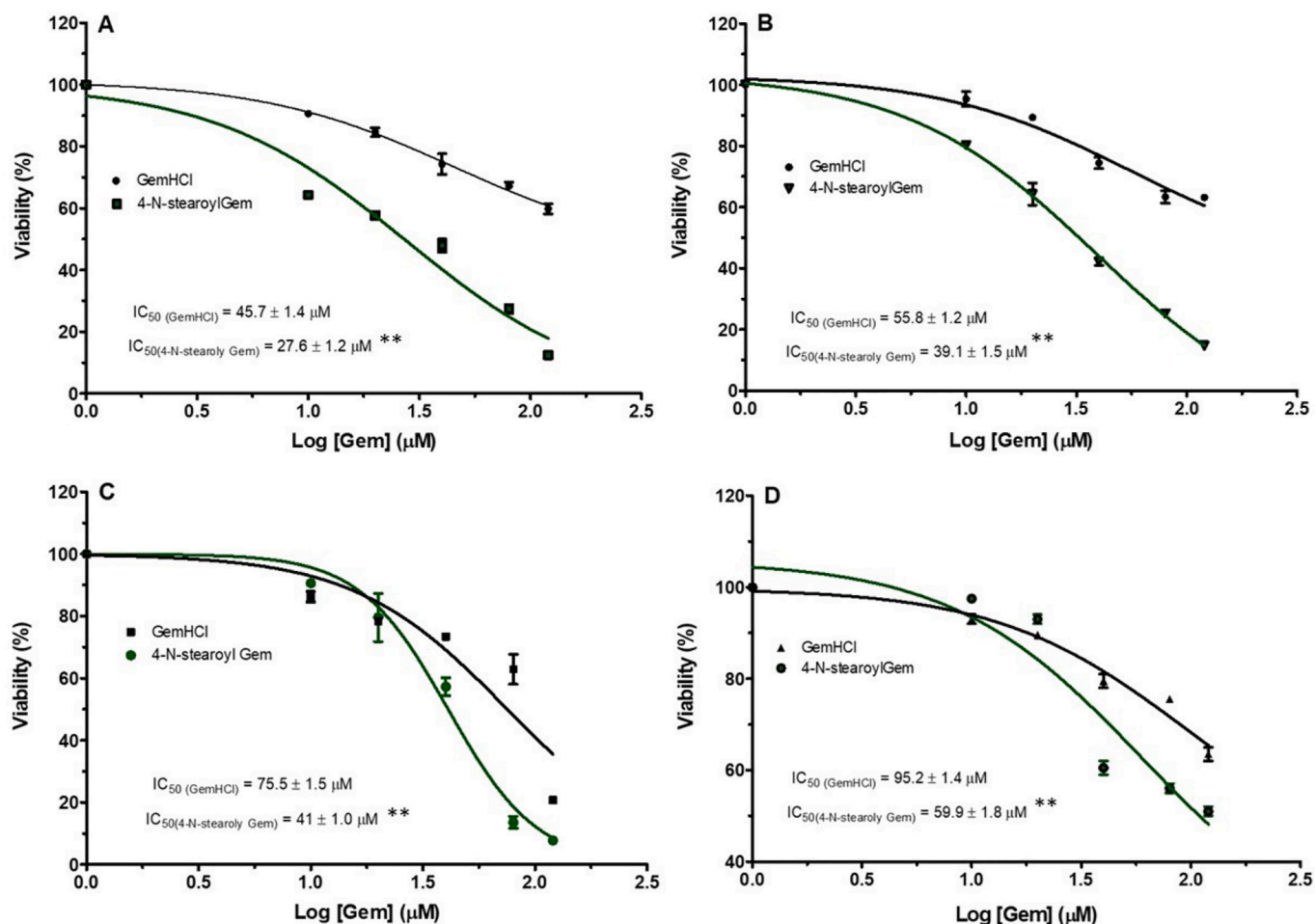
Fig. 1. Cytotoxic activity of GemHCl and 4NSG on MiaPaCa-2 cells and PPCL-46 cells at varying concentrations. Cytotoxic studies on (A) MiaPaCa-2 (2D culture) treated with GemHCl and 4NSG, (B) Mia-PaCa-2 (3D culture) treated with GemHCl and 4NSG, (C) PPCL-46 (2D culture) treated with GemHCl and 4NSG, (D) PPCL-46 (3D culture) treated with GemHCl and 4NSG. IC_{50} values for 4NSG were significantly lower compared to corresponding values for GemHCl which implies that 4NSG has higher cytotoxic activity against MiaPaCa-2 and PPCL-46 (2D and 3D) cultures compare to that of GemHCl. Data represent mean $\pm$ SEM, $n = 3$. $p < 0.01$ (**) (GemHCl $_{(IC50)}$ vs 4NSG$_{(IC50)}$).

Table 1

IC_{50} values of GemHCl and 4NSG treated MiaPaCa-2 and PPCL-46 2D and 3D cultures.

	IC_{50} μM (2D MiaPaCa-2 culture)	IC_{50} μM (3D MiaPaCa-2 culture)
GemHCl	45.7 ± 1.4	55.8 ± 1.2
4NSG	27.6 ± 1.3**	39.1 ± 1.5**

	IC_{50} μM (2D PPCL-46 culture)	IC_{50} μM (3D PPCL-46 culture)
GemHCl	75.5 ± 1.9	95.2 ± 1.4
4NSG	41.1 ± 2.3**	59.9 ± 1.8**

Data represents mean $\pm$ SEM, n = 3. p < 0.01(**)(GemHCl $_{(IC50)}$ vs 4NSG$_{(IC50)}$).

GemHCl treated tumors exhibited significant VEGF receptor expression (IHC 3 +) Fig. 5G and H, while 4NSG treated tumor caused significant decrease in VEGF receptor expression (IHC 0) showing only trace immunostaining (Fig. 5I).

3.6. Tumor efficacy studies

In the 4NSG treated group, a significant tumor growth suppression was observed compared with the control or GemHCl group (Fig. 6A). While the mean tumor volume of the control group was extremely large, the mean tumor volume of 4NSG group exhibited significantly lower tumor growth compared with the mean tumor volume of GemHCl group especially on the 35th day through to 46th day. Fig. 6B shows that terminal tumor weight of the 4NSG treated group was significantly reduced compared with control or GemHCl treated group. Fig. 6C shows images of tumor extracted from control, GemHCl and 4NSG groups on day 46. Examination of the tumor images clearly shows that 4NSG group had the smallest size followed by the GemHCl group, and lastly the control group (non-treated).

The weights of the mice were monitored during the entire study and changes in the mice weights are shown in Fig. 6D. With the initial normalized body weight at 100%, we observed that the normalized body weight of control mice-bearing tumors ranged from 100% to 104% with 4% increase in body weight. While normalized body weight of GemHCl and 4NSG treated mice bearing tumors ranged from 94.5% to 100% with 4.5% decrease in body weight.

4. Discussion

Data from numerous researches with commercially available PCa cells have demonstrated the effectiveness of Gem loaded nanoparticles to significantly suppress tumor growth and supposedly overcome resistance. For emphasis, these monogenous cell lines lack predictive value but their importance cannot be damped as they still have relevance in preliminary screening of anti-cancer agents. This has
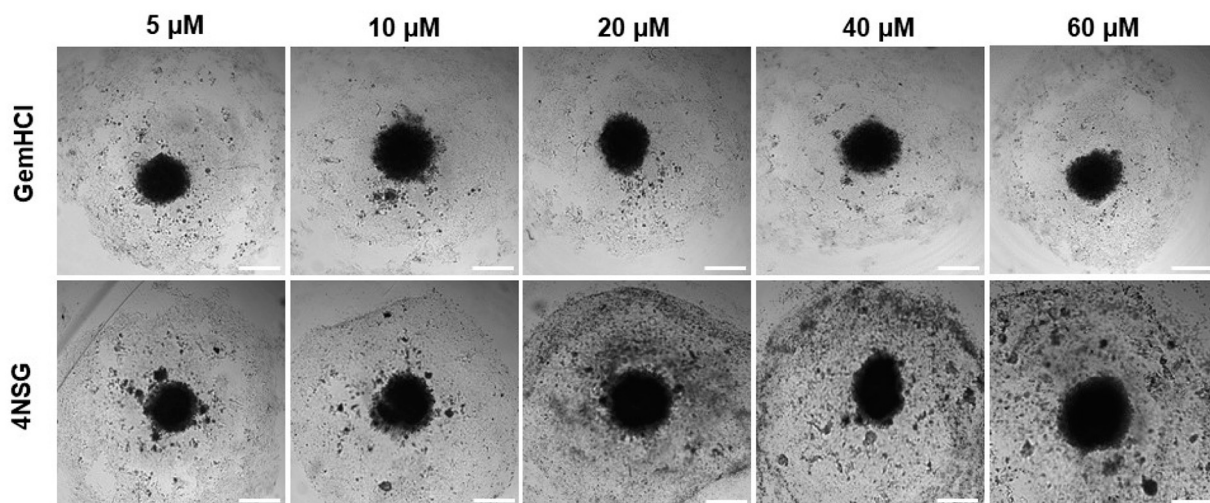
Fig. 2. PPCL-46 spheroidal integrity after treatment with GemHCl and 4NSG at different concentrations. The 4NSG treated PPCL-46 spheroids exhibited irregular or non-spheroidal shapes with increased spheroidal surface area as 4NSG concentration increases. While GemHCl treated spheroids were observed to have a smaller surface spheroidal area with less non-spheroidal shapes. Appearance of non-spheroidal shapes clearly indicates spheroids disruption and a reflection of cell loss due to high anticancer activity due to 4NSG compared with GemHCl.
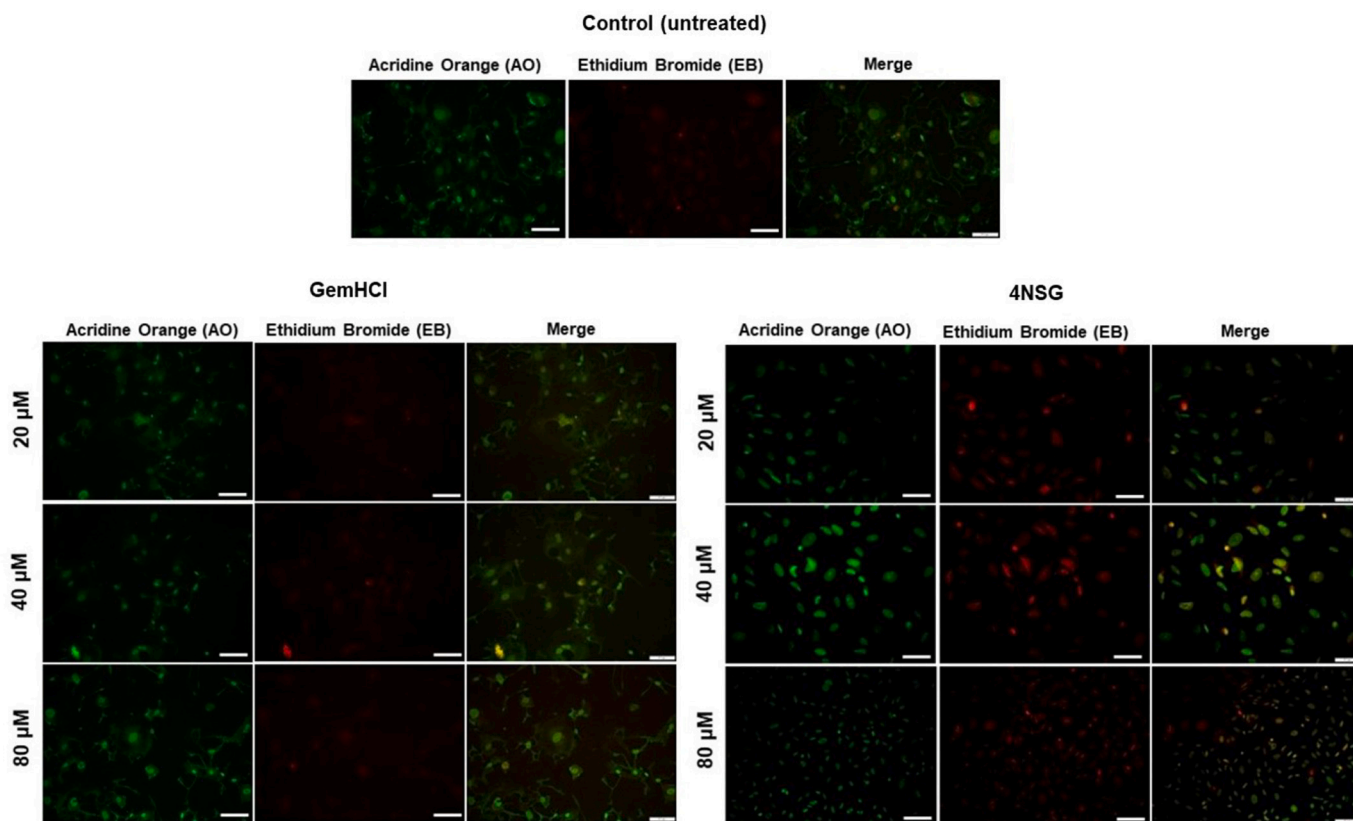

Fig. 3. Apoptosis studies of on PPCL-46 cells exposed to GemHCl and 4NSG at different concentrations was performed by staining with acridine orange/ethidium bromide in GemHCl and 4NSG (fluorescence microscopy magnification of 20×). At higher concentrations (40 μM and 80 μM), 4NSG treated PPCL-46 cells showed signs of early apoptosis illustrated as greenish yellow florescence compared with GemHCl (merged images). Late apoptosis was identified as reddish-orange fluorescence in 4NSG treated cells compared with the control or GemHCl treated cells at Gem concentrations at 20 and 40 μM. (For interpretation of the references to colour in this figure legend, the reader is referred to the web version of this article.)

necessitated the need to employ patient PPCL-46 with a higher predictive value (Hidalgo et al., 2014; Jin et al., 2010). In this preliminary study, we underscore the importance and benefit of utilizing a 4NSG (Gem conjugate) for both in-vitro and in-vivo studies in PPCL-46 in lieu of commercially available counterparts. It is worthwhile to note that others have demonstrated the effectiveness of some Gem analogs in

myriad of commercially available cell lines (Immordino et al., 2004; Chung et al., 2012).

Prior to in vitro studies, the structure and purity of 4NSG was confirmed using NMR and elemental analysis (Supplementary Fig. S1 A and B, Supplementary Fig. S2). In fact, the purity of the 4NSG was 99.6% suggesting that the synthesized compound used in this study was
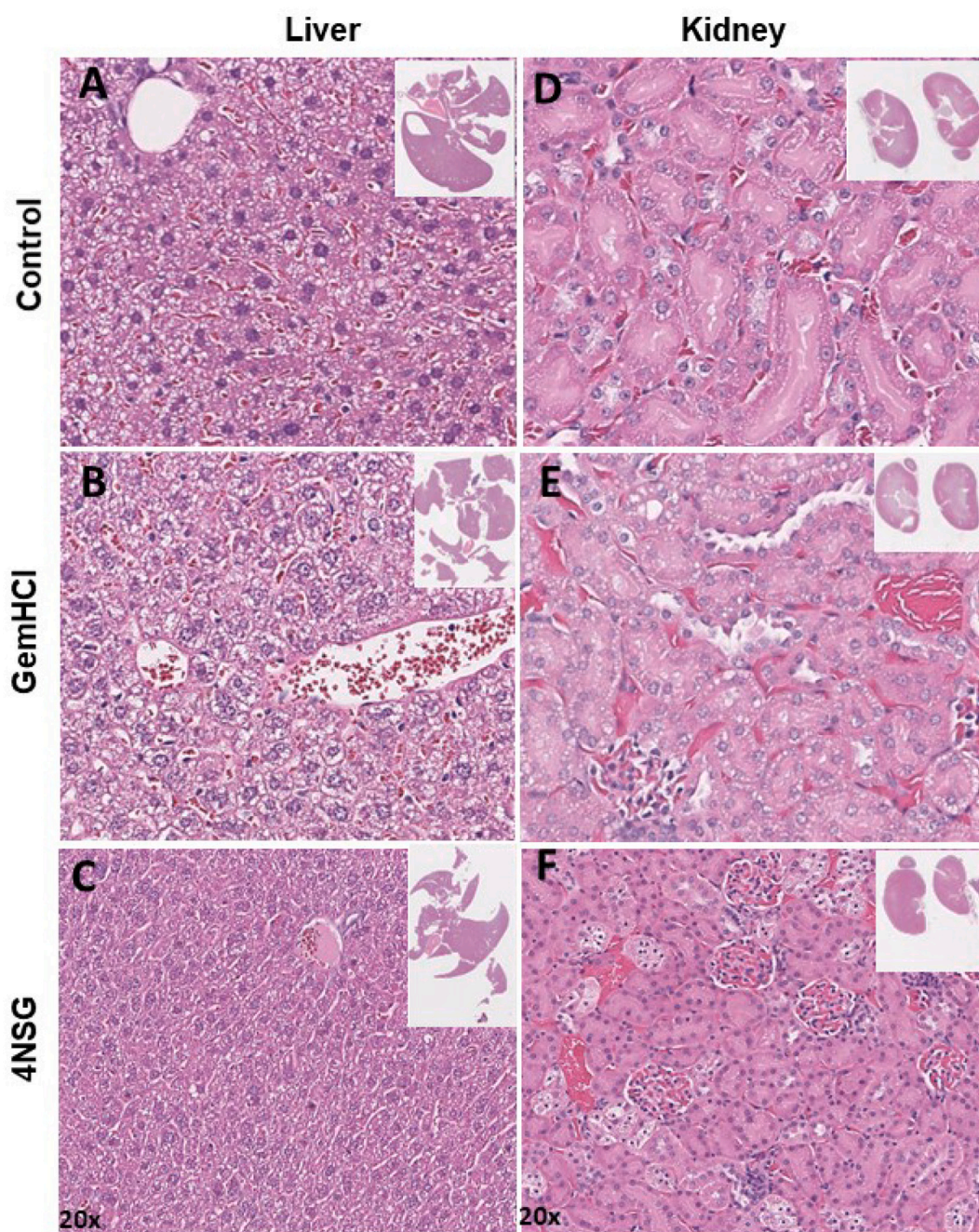
Fig. 4. Transverse section (evaluated by H&E staining) through the liver and kidney extracted from mice after 7 days post injection with 50 mg/kg of GemHCl and 30 mg/kg of Gem equivalent in 4NSG. Hemotoxilin-Eosin (H&E) staining of the liver of A) control, B) GemHCl, C) 4NSG. H&E staining of the kidney of D) Control, E) GemHCl, F) 4NSG. Magnification: 20×.

significantly devoid of any unwanted material. As shown in Fig. 1, IC_{50} values for 4NSG were significantly lower than corresponding values for GemHCl which implies that 4NSG has higher antiproliferation activity against 2D and 3D MiaPaCa-2 and PPCL-46 cultures. The unique characteristics of 4NSG that might have been attributed to its high anticancer activity was probably due to modification of the polar nature of GemHCl to moderately lipophilic through conjugation of Gem to stearic acid. In addition, Gem has been reported to rely heavily on nucleoside transporters (hENT1) for its delivery and accumulation into PCa cells and under-expression of these transporters has been demonstrated to confer resistance of PCa (Wonganan et al., 2013). Owing to 4NSG lipophilicity nature, we suggest that it may enter PCa cell by passive diffusion and evidence of such mechanism of transport is

provided by works done by others using Gem derivatives (Bildstein et al., 2010). It has been demonstrated that hydrolytic enzymes such as fatty acid amide hydrolases (FAAH) ubiquitous in intracellular membrane and confined in endothelium reticulum (ER) facilitates the release of Gem from 4NSG by cleaving the amide linkage (Wonganan et al., 2013; Arreaza and Deutsch, 1999). The released Gem is actively converted to the metabolite, Gem triphosphate which blocks DNA synthesis when delivered to the appropriate intracellular compartment implicated in phosphorylation process (Wonganan et al., 2013). In contrast, the weak cytotoxicity effect of GemHCl against 2D and 3D cultures could be attributed to inefficient transportation across cell membrane as a result of rapid deamination of GemHCl and under-expression of transporters (Chen et al., 2018). Indeed, we admit that
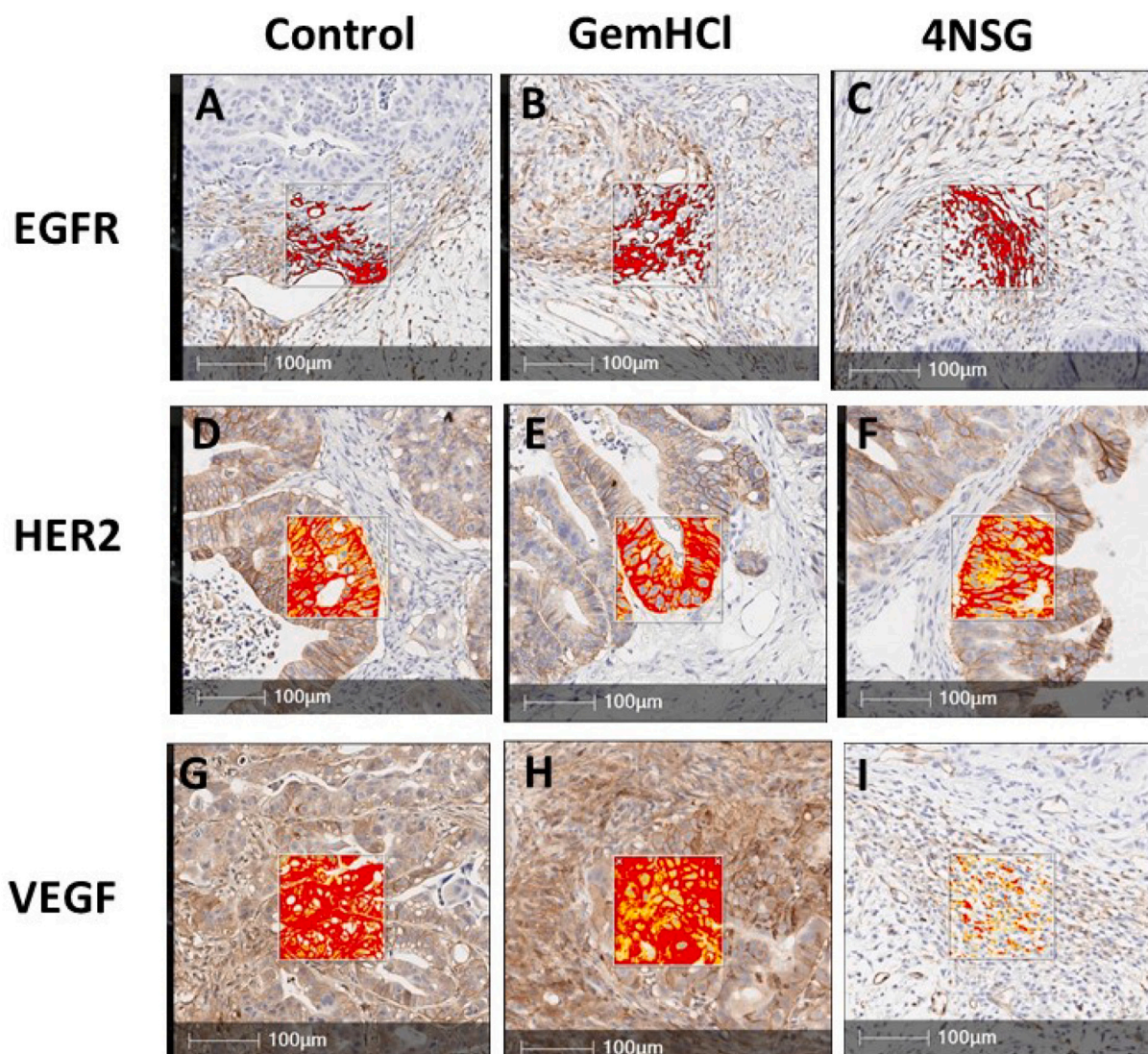
Fig. 5. Immunohistochemical staining of EGFR, HER2 and VEGF in PDX tumor sections. Regions (brown areas) demonstrate high positive staining. Images A, B and C show moderate EGFR expression (IHC 1+), images D, E and F demonstrate high HER2 expression (IHC 2+), G and H images show overexpression of VEGF overexpression (IHC 3+) and image I shows negative staining for VEGF (IHC 0). The boxed areas illustrate higher magnification of the tumor sections. (For interpretation of the references to colour in this figure legend, the reader is referred to the web version of this article.)

Table 2

Quantitative determination of liver enzymes profile in serum after administration of GemHCl and 4NSG in mice bearing subcutaneous PPCL-46 tumor.

Parameter	Control	GemHCl	4NSG
ALT (mUnits/mL)	67 ± 5	232 ± 28 *	172 ± 22
AST (mUnits/mL)	62 ± 13	85 ± 9	76 ± 18

Data represents mean $\pm$ SD, n = 3. p-value = 0.04* (GemHCl$_{ALT}$ vs 4NSG$_{ALT}$), p-value = 0.70 (GemHCl$_{AST}$ vs 4NSG$_{AST}$). p* < 0.05 is considered significant.

hydrolysis of 4NSG to release Gem can occur intracellularly outside the compartment for phosphorylation hence diminishing the efficacy of 4NSG as it suffers from possible intracellular deamination prior to phosphorylation to a certain degree after the release of Gem. After the hydrolysis of the amide bond intracellularly, there is also the possibility of Gem efflux prior to delivery to phosphorylation enzymes (Chen et al., 2018). The current study tentatively cast a new light on extensive cellular uptake and efficacy of 4NSG than GemHCl. Furthermore, cell induced death or apoptotic studies further support our assertion that 4NSG exhibited a strong cytotoxic effect compared with GemHCl.

Table 3

Pharmacokinetic profiles of after GemHCl and 4NSG were administered intravenously to mice.

Parameter	Unit	One-compartment model		Significance level p-value
		GemHCl	4NSG	
K_{10}	1/h	1.01 ± 0.03	0.36 ± 0.04	0.0001
$t_{1/2}$	h	0.70 ± 0.01	1.93 ± 0.06	0.0001
V_d	mL	21.7 ± 1.9	19.3 ± 0.2	0.3619
CL	mL/h	21.3 ± 3.2	7.1 ± 1.1	0.0001
AUC $_{(0-t)}$	µg/(mL * h)	28.2 ± 4.3	86.2 ± 5.4	0.0001
AUMC$_{(0-inf)}$	µg/(mL * h^2)	28.2 ± 4.1	86.6 ± 4.8	0.0001
MRT	h	1.2 ± 0.1	2.8 ± 0.4	0.02
V_{ss}	µg/(µg/mL)	21.7 ± 3.6	23.9 ± 1.6	ns

k_{10}, elimination rate constant; $t_{1/2}$, half-life; AUC$_{(0-t)}$, area under the plasma concentration–time curve; AUMC$_{(0-inf)}$, area under the first moment curve; MRT, mean residence time; Cl, clearance; V_d, volume of distribution; V_{ss}, volume of distribution at steady state. (Data analyzed using t-test).
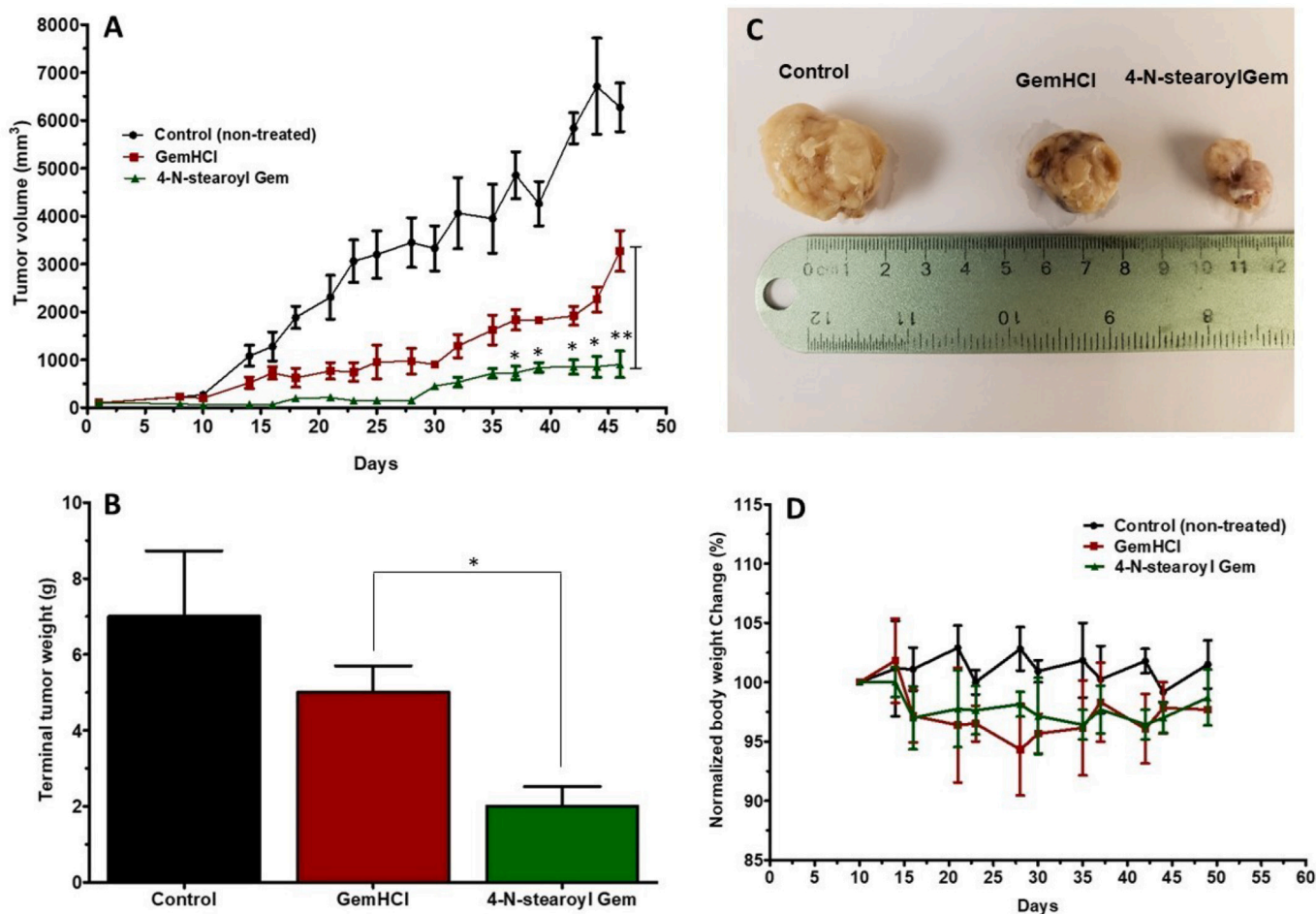
Fig. 6. In-vivo efficacy of 4NSG in PDX mouse model. Tumor growth curves of GemHCl and 4NSG treated mice bearing pancreatic PDX tumor (A), Terminal tumor weight of treated mice (B), Picture of tumors harvested from control, GemHCl and 4NSG treated mice (C), mouse body weight changes during treatment (D). Asterisks represent level of significance between control and treatment group (*$p < 0.05$, **$p < 0.01$). All data represents mean ± SD, (n = 6/group).

While AST enzyme level appears to be transiently elevated in GemHCl group, ALT enzyme levels in GemHCl and 4NSG groups were significantly high compared with the control. But these levels did not affect the integrity of the liver as pathological examination of the liver tissues revealed no observable damage in these treatment groups. In addition to this, we observed no noticeable damage in kidney tissues of mice treated with GemHCl and 4NSG. Our findings are supported in part by similar works carried out by other researchers where no noticeable acute or subacute liver toxicity was observed post intravenous injection of mice treated with Gem conjugates (Sloat et al., 2011). Put together, mouse body weight change, liver enzymes levels and pathological data of liver and kidney of 4NSG was not different from the control PDX mice. This demonstrates that 4NSG exhibited no observable toxic effect in the PDX mouse model.

EGFR, HER2 and VEGF are tyrosine kinase receptors highly expressed in several solid tumors including PCa (Lozano-Leon et al., 2011; Karanikas et al., 2016). These receptors are frequently reported to harbor aberrant activities that lead to the proliferation, survival, migration and differentiation required for PCa pathogenesis. In this study, we investigated the effects of GemHCl and 4NSG on the expressions of EGFR, HER2 and VEGFR in PDX mouse model bearing pancreatic tumor. In this particular PDX model, high expressions of EGFR and HER2 were observed after IHC staining tumor of GemHCl and 4NSG treated groups suggesting that GemHCl and 4NSG may not effectively be used as EGFR or HER2 targeted therapy. A similar study was preformed where exposure of PCa cells to Gem resulted in increased

phosphorylation and activation of EGFR (Morgan et al., 2008). In addition, a major partner of EGFR, HER-2 has been reported to be overexpressed in numerous human cancers with associated multiple drug resistance (Friess et al., 1996). While there was no significant difference in VEGF receptor expression between control (IHC 3+) and GemHCl treated (IHC 3+) tumor tissues, treatment with 4NSG resulted in reduction of VEGF receptor expression (trace or negative). Based on this, we could suggest that treatment with 4NSG may have resulted in significant reduction in the tumor growth and is most likely due to 4NSG's ability to target VEGF receptors.

Anti-tumor activity of 4NSG after the 30th day exhibited a significant inhibition of tumor growth compared with GemHCl. And three major factors could be used to explain the extraordinary tumor efficacy of 4NSG: i) absence of free NH_2-group on 4NSG which rendered the cysteine deaminase enzyme ineffective to metabolize Gem. This event most likely allowed for prolong circulation, increased bioavailability and improved therapeutic efficacy of 4NSG ii) 4NSG ability to significantly inhibit VEGR receptor expression and iii) conjugation of Gem to stearic acid may have imparted some degree of lipophilicity to 4NSG which may have facilitated its delivery to cancer cells.

5. Conclusion

In this study, we demonstrated that synthesized 4NSG remarkably reduced tumor growth in pancreatic PDX mouse model due to increased bioavailability and reduced VEGF receptors expression. Toxicological

profile of 4NSG was not distinct from control (non-treated) PDX mice. To improve significantly the in-vivo efficacy of 4NSG, our future studies would involve the design, development and optimization of targeted 4NSG PEGylated nanoparticles.

Data availability

The data will be made available upon request.

Declaration of Competing Interest

The authors declare that they have no known competing financial interests or personal relationships that could have appeared to influence the work reported in this paper.

Acknowledgements

Appendix A. Supplementary data

Supplementary data to this article can be found online at https://doi.org/10.1016/j.ijpx.2020.100056.

References

Affram, K., et al., 2017. Smart thermosensitive liposomes for effective solid tumor therapy and in vivo imaging. PLoS One 12, e0185116. https://doi.org/10.1371/journal.pone.0185116.

Amrutkar, M., Gladhaug, I.P., 2017. Pancreatic cancer chemoresistance to Gemcitabine. Cancers (Basel) 9. https://doi.org/10.3390/cancers9110157.

Andersson, R., 2009. Gemcitabine chemoresistance in pancreatic cancer: molecular mechanisms and potential solutions. Scand. J. Gastroenterol. 44, 782–786. https://doi.org/10.1080/00365520902745039.

Apparaju, S.K., Gudelsky, G.A., Desai, P.B., 2008. Pharmacokinetics of gemcitabine in tumor and non-tumor extracellular fluid of brain: an in vivo assessment in rats employing intracerebral microdialysis. Cancer Chemother. Pharmacol. 61, 223–229. https://doi.org/10.1007/s00280-007-0464-1.

Arreaza, G., Deutsch, D.G., 1999. Deletion of a proline-rich region and a transmembrane domain in fatty acid amide hydrolase. FEBS Lett. 57–60.

Beumer, J.H., et al., 2008. Modulation of gemcitabine (2′,2′-difluoro-2′-deoxycytidine) pharmacokinetics, metabolism, and bioavailability in mice by 3,4,5,6-tetrahydrouridine. Clin. Cancer Res. 14, 3529–3535. https://doi.org/10.1158/1078-0432.CCR-07-4885.

Bildstein, L., et al., 2010. Transmembrane diffusion of gemcitabine by a nanoparticulate squalenoyl prodrug: an original drug delivery pathway. J. Control. Release 147, 163–170. https://doi.org/10.1016/j.jconrel.2010.07.120.

Binenbaum, Y., Na'ara, S., Gil, Z., 2015. Gemcitabine resistance in pancreatic ductal adenocarcinoma. Drug Resist. Updat. 23, 55–68. https://doi.org/10.1016/j.drup.2015.10.002.

Chen, Z., Zheng, Y., Shi, Y., Cui, Z., 2018. Overcoming tumor cell chemoresistance using nanoparticles: lysosomes are beneficial for (stearoyl) gemcitabine-incorporated solid lipid nanoparticles. Int. J. Nanomedicine 13, 319–336. https://doi.org/10.2147/IJN.S149196.

Chung, W.G., Sandoval, M.A., Sloat, B.R., Lansakara, P.D., Cui, Z., 2012. Stearoyl gemcitabine nanoparticles overcome resistance related to the over-expression of ribonucleotide reductase subunit M1. J. Control. Release 157, 132–140. https://doi.org/10.1016/j.jconrel.2011.08.004.

Dai, J.-T., et al., 2017. Enhancement of gemcitabine against pancreatic cancer by loading in mesoporous silica vesicles. Chin. Chem. Lett. 28, 531–536. https://doi.org/10.1016/j.cclet.2016.11.008.

de Sousa Cavalcante, L., Monteiro, G., 2014. Gemcitabine: metabolism and molecular mechanisms of action, sensitivity and chemoresistance in pancreatic cancer. Eur. J. Pharmacol. 741, 8–16. https://doi.org/10.1016/j.ejphar.2014.07.041.

Delitto, D., et al., 2015. Patient-derived xenograft models for pancreatic adenocarcinoma demonstrate retention of tumor morphology through incorporation of murine stromal elements. Am. J. Pathol. 185, 1297–1303. https://doi.org/10.1016/j.ajpath.2015.01.016.

Diaz Osterman, C.J., et al., 2016. Curcumin Induces Pancreatic Adenocarcinoma Cell Death Via Reduction of the Inhibitors of Apoptosis. Pancreas 45, 101–109. https://doi.org/10.1097/MPA.0000000000000411.

Friess, H., et al., 1996. Pancreatic cancer: the potential clinical relevance of alterations in growth factors and their receptors. J. Mol. Med. (Berl) 74, 35–42. https://doi.org/10.1007/BF00202070.

Garcia-Cremades, M., Pitou, C., Iversen, P.W., Troconiz, I.F., 2018. Predicting tumour growth and its impact on survival in gemcitabine-treated patients with advanced pancreatic cancer. Eur. J. Pharm. Sci. 115, 296–303. https://doi.org/10.1016/j.ejps.2018.01.033.

Gradiz, R., Silva, H.C., Carvalho, L., Botelho, M.F., Mota-Pinto, A., 2016. MIA PaCa-2 and PANC-1 - pancreas ductal adenocarcinoma cell lines with neuroendocrine differentiation and somatostatin receptors. Sci. Rep. 6, 21648. https://doi.org/10.1038/srep21648.

Grasso, C., Jansen, G., Giovannetti, E., 2017. Drug resistance in pancreatic cancer: impact of altered energy metabolism. Crit. Rev. Oncol. Hematol. 114, 139–152. https://doi.org/10.1016/j.critrevonc.2017.03.026.

Harder, J., et al., 2009. EGFR and HER2 expression in advanced biliary tract cancer. World J. Gastroenterol. 15, 4511–4517. https://doi.org/10.3748/wjg.15.4511.

Hidalgo, M., et al., 2014. Patient-derived xenograft models: an emerging platform for translational cancer research. Cancer Discov. 4, 998–1013. https://doi.org/10.1158/2159-8290.CD-14-0001.

Immordino, M.L., et al., 2004. Preparation, characterization, cytotoxicity and pharmacokinetics of liposomes containing lipophilic gemcitabine prodrugs. J. Control. Release 100, 331–346. https://doi.org/10.1016/j.jconrel.2004.09.001.

Jia, Y., Xie, J., 2015. Promising molecular mechanisms responsible for gemcitabine resistance in cancer. Genes Dis. 2, 299–306. https://doi.org/10.1016/j.gendis.2015.07.003.

Jin, K., et al., 2010. Patient-derived human tumour tissue xenografts in immunodeficient mice: a systematic review. Clin. Transl. Oncol. 12, 473–480. https://doi.org/10.1007/s12094-010-0540-6.

Karanikas, M., et al., 2016. Pancreatic cancer from molecular pathways to treatment opinion. J. Cancer 7, 1328–1339. https://doi.org/10.7150/jca.15419.

Krishna, M., 2013. Role of special stains in diagnostic liver pathology. Clin Liver Dis (Hoboken) 2, S8–S10. https://doi.org/10.1002/cld.148.

Kumar, B.S., et al., 2014. Development and characterization of lecithin stabilized glibenclamide nanocrystals for enhanced solubility and drug delivery. Drug Deliv. 21, 173–184. https://doi.org/10.3109/10717544.2013.840690.

Lanz, C., Fruh, M., Thormann, W., Cerny, T., Lauterburg, B.H., 2007. Rapid determination of gemcitabine in plasma and serum using reversed-phase HPLC. J. Sep. Sci. 30, 1811–1820. https://doi.org/10.1002/jssc.200600534.

Li, X.M., et al., 2005. Preclinical relevance of dosing time for the therapeutic index of gemcitabine-cisplatin. Br. J. Cancer 92, 1684–1689. https://doi.org/10.1038/sj.bjc.6602564.

Liu, K., Liu, P.C., Liu, R., Wu, X., 2015. Dual AO/EB staining to detect apoptosis in osteosarcoma cells compared with flow cytometry. Med. Sci. Monit. Basic Res. 21, 15–20. https://doi.org/10.12659/MSMBR.893327.

Liu, Y., Tamam, H., Yeo, Y., 2018. Mixed liposome approach for ratiometric and sequential delivery of paclitaxel and gemcitabine. AAPS PharmSciTech 19, 693–699. https://doi.org/10.1208/s12249-017-0877-z.

Lozano-Leon, A., et al., 2011. Ductal adenocarcinoma of the pancreas: Expression of growth factor receptors, oncogenes and suppressor genes, and their relationship to pathological features, staging and survival. Oncol. Lett. 2, 161–166. https://doi.org/10.3892/ol.2010.206.

Mei, L., Du, W., Ma, W.W., 2016. Targeting stromal microenvironment in pancreatic ductal adenocarcinoma: controversies and promises. J Gastrointest Oncol. 7, 487–494. https://doi.org/10.21037/jgo.2016.03.03.

Morgan, M.A., et al., 2008. The combination of epidermal growth factor receptor inhibitors with gemcitabine and radiation in pancreatic cancer. Clin. Cancer Res. 14, 5142–5149. https://doi.org/10.1158/1078-0432.CCR-07-4072.

Paskeviciute, M., Petrikaite, V., 2017. Differences of statin activity in 2D and 3D pancreatic cancer cell cultures. Drug Des. Devel. Ther. 11, 3273–3280. https://doi.org/10.2147/DDDT.S149411.

Pham, K., et al., 2016. Isolation of pancreatic cancer cells from a patient-derived xenograft model allows for practical expansion and preserved heterogeneity in culture. Am. J. Pathol. 186, 1537–1546. https://doi.org/10.1016/j.ajpath.2016.02.009.

Pignochino, Y., et al., 2010. Targeting EGFR/HER2 pathways enhances the antiproliferative effect of gemcitabine in biliary tract and gallbladder carcinomas. BMC Cancer 10, 631. https://doi.org/10.1186/1471-2407-10-631.

Popescu, R.C., et al., 2017. Fabrication and cytotoxicity of gemcitabine-functionalized magnetite nanoparticles. Molecules 22. https://doi.org/10.3390/molecules22071080.

Ricart, A.D., 2017. Drug-induced liver injury in Oncology. Ann. Oncol. 28, 2013–2020. https://doi.org/10.1093/annonc/mdx158.

Siegel, R.L., Miller, K.D., Jemal, A., 2019. Cancer statistics, 2019. CA Cancer J. Clin. 69, 7–34. https://doi.org/10.3322/caac.21551.

Sloat, B.R., et al., 2011. In vitro and in vivo anti-tumor activities of a gemcitabine derivative carried by nanoparticles. Int. J. Pharm. 409, 278–288. https://doi.org/10.1016/j.ijpharm.2011.02.037.

Trung Bui, D., et al., 2013. Polymer prodrug nanoparticles based on naturally occurring isoprenoid for anticancer therapy. Biomacromolecules 14, 2837–2847. https://doi.org/10.1021/bm400657g.

Vande Voorde, J., et al., 2019. Improving the metabolic fidelity of cancer models with a physiological cell culture medium. Sci. Adv. 5 https://doi.org/10.1126/sciadv.aau7314. eaau7314.

Walsh, N., et al., 2013. EGFR and HER2 inhibition in pancreatic cancer. Investig. New Drugs 31, 558–566. https://doi.org/10.1007/s10637-012-9891-x.

Wen, Z., et al., 2013. A spheroid-based 3-D culture model for pancreatic cancer drug testing, using the acid phosphatase assay. Braz. J. Med. Biol. Res. 46, 634–642. https://doi.org/10.1590/1414-431X20132647.

Wonganan, P., et al., 2013. Just getting into cells is not enough: mechanisms underlying 4-(N)-stearoyl gemcitabine solid lipid nanoparticle's ability to overcome gemcitabine resistance caused by RRM1 overexpression. J. Control. Release 169, 17–27. https://doi.org/10.1016/j.jconrel.2013.03.033.

Zhang, Y., Huo, M., Zhou, J., Xie, S., 2010. PKSolver: an add-in program for pharmacokinetic and pharmacodynamic data analysis in Microsoft Excel. Comput. Methods Prog. Biomed. 99, 306–314. https://doi.org/10.1016/j.cmpb.2010.01.007.

Zhang, X., Xing, H., Zhao, Y., Ma, Z., 2018. Pharmaceutical dispersion techniques for dissolution and bioavailability enhancement of poorly water-soluble drugs. Pharmaceutics 10. https://doi.org/10.3390/pharmaceutics10030074.